Effects of bone density alterations on strain patterns in the pelvis: application of a finite element model

A S O Leung, L M Gordon, T Skrinskas, T Szwedowski, and **C M Whyne***
Orthopaedic Biomechanics Laboratory, Sunnybrook Health Sciences Centre, Toronto, Ontario, Canada

The manuscript was received on 19 March 2009 and was accepted after revision for publication on 26 June 2009.

DOI: 10.1243/09544119JEIM618

Abstract: Insufficiency fractures occur when physiological loads are applied to bone deficient in mechanical resistance. A better understanding of pelvic mechanics and the effect of bone density alterations could lead to improved diagnosis and treatment of insufficiency fractures. This study aimed to develop and validate a subject-specific three-dimensional (3D) finite element (FE) model of a pelvis, to analyse pelvic strains as a function of interior and cortical surface bone density, and to compare high strain regions with common insufficiency fracture sites. The FE model yielded strong agreement between experimental and model strains. By means of the response surface method, changes to cortical surface bone density using the FE model were found to have a 60 per cent greater influence compared with changes in interior bone density. A small interaction was also found to exist between surface and interior bone densities (<3 per cent), and a non-linear effect of surface bone density on strain was observed. Areas with greater increases in average principal strains with reductions in density in the FE model corresponded to areas prone to insufficiency fracture. Owing to the influence of cortical surface bone density on strain, it may be considered a strong global (non-linear) indicator for insufficiency fracture risk.

Keywords: pelvis, finite element modelling, experimental validation, bone density, insufficiency fracture, response surface

1 INTRODUCTION

The pelvis in the human musculoskeletal system serves as a transfer point for upper body loads to the lower extremities. The stability of the pelvic ring structure, which contains slightly movable articulations such as the symphysis pubis and the sacroiliac joints, depends on the posterior weight-bearing sacroiliac complex together with the sacroiliac, sacrotuberous, and sacrospinous ligaments [**1**]. It is composed of flat bones consisting of low-density trabecular bone tissue on the interior covered by a thin layer of higher-density cortical bone on the surface [**2**, **3**]. Although it is an optimal composite material with low weight and high strength, this structure is very sensitive to fractures.

**Corresponding author: Orthopaedic Biomechanics Laboratory, Sunnybrook Health Sciences Centre, 2075 Bayview Avenue, Toronto, Ontario, M4N 3M5, Canada.*
email: cari.whyne@sunnybrook.ca; annie.so.leung@gmail.com

Stress fractures occur owing to repetitive, prolonged muscular action on a bone that lacks the mechanical elasticity to resist the load. They are categorized into fatigue fractures, which are abnormal loads to a normal bone, and insufficiency fractures, which are normal loads to a bone deficient in mineral or mechanical resistance owing to structural alterations of the bone [**4**, **5**]. Mechanical resistance, or bone quality, is quantified by bone mineral density (BMD) as well as structural geometry, which determine the way stresses produced by loading forces are transmitted through the bone. Both men and women experience age-related decrease in trabecular bone density and toughness of cortical bone, which contributes to osteoporotic fragility and increased fracture risk [**6**–**11**]. It has been shown that bony geometry also influences fracture risk owing to associated changes in structural strength, loading, and contact forces [**12**, **13**].

The most common insufficiency fracture locations in the body are the pelvic ring (30.7 per cent) and the

Downloaded from pih.sagepub.com at UNIV TORONTO on January 12, 2012

sacrum (29.6 per cent) [**14**]. The three predominant iliac insufficiency fracture sites are (1) supra-acetabular, above and parallel to the acetabular roof, (2) oblique iliac, extending diagonally across the iliac ala from the greater sciatic notch, and (3) superomedial iliac, adjacent to the sacroiliac joint [**15**]. Insufficiency fractures have also been reported in both superior and inferior pubic rami, which are frequently associated with concurrent fractures in the sacrum [**16**, **17**]. In sacral insufficiency fractures, the majority run vertically, parallel to the sacroiliac joint, approximately in line with the lateral margins of the lumbar vertebrae and the vertical loading axis [**18**–**23**]. Figure 1 highlights these vulnerable sites. Risk factors for pelvic insufficiency fractures include osteoporosis, rheumatoid arthritis, osteomalacia, radiotherapy, and mechanical constraint resulting from total hip replacement. All these factors result in bone demineralization and thus decreased strength and elasticity of the pelvic bone. Clinical symptoms of pelvic insufficiency fractures include lower back pain, groin pain, and ill-defined pains of the lower limbs, all of which may produce limping or functional disability of joint movement [**14**].

While reduced mechanical resistance in the pelvis has been established as a major risk factor for insufficiency fractures, little is known about the specific impact of changes in density and geometry on strain patterns in the pelvis under normal physiological loads. A better understanding of pelvic mechanics and the effect of changes in mechanical and geometric properties of the pelvic bone could lead to improved diagnosis, treatment, and alleviation of symptoms associated with pelvic insufficiency fractures.

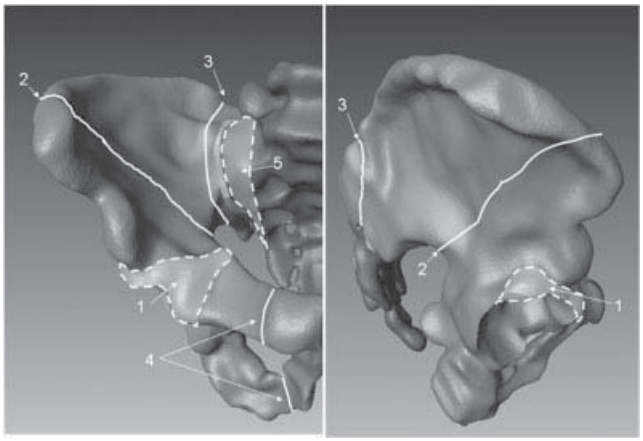

Fig. 1 Common insufficiency fracture sites in the pelvis. In the ilium, insufficiency fracture sites are found in the supra-acetabular (1), oblique iliac (2), and superomedial iliac (3) regions. Superior and inferior pubic rami (4) as well as zone 1 of the sacrum as defined by Denis *et al.* (5) are also sites prone to insufficiency fractures

Strain distributions in the pelvis have been assessed experimentally using strain gauging techniques; however, these measures only provide strains at discrete locations and are not suitable for parametric analyses [**24**–**27**]. The use of simplified mathematical models is limited by the geometrical and material property complexity of the pelvic structure. Finite element (FE) analysis is a computational modelling technique that has been successfully used to provide information on strain and stress patterns in complex bony structures including the pelvis [**24**–**32**]. FE models have been validated through mechanical testing, which demonstrates that, given accurate geometries, material data, and boundary conditions, the FE method can be used reliably to predict the strength of healthy and pathologic bones. Subject-specific FE models have been developed with the aid of current medical imaging techniques to analyse complex geometries and complicated constitutive behaviours, such as the heterogeneous, non-linear, and anisotropic material property distributions for bone, which can be quantified using computed tomography (CT) intensity data [**24**, **25**]. Numerous FE models have been developed for the pelvis, but the majority have not been validated experimentally [**33**–**37**]. The subset of models that have been experimentally validated were run under either non-physiological conditions or in a simulated single-leg stance position [**24**–**27**].

Parametric analyses of FE models can be utilized to determine the impact of specific factors, including material properties, loading and boundary conditions, and geometry, on model outcome variables. However, optimization of parameter selection to enhance modelling efforts in the analysis of bony structures has been limited. The response surface method (RSM) is a statistical tool used for optimizing a response variable by finding the optimal values of two or more independent parameters, and has been widely used in structural analysis and pharmaceutical experimental design [**38**, **39**]. The RSM is directly applicable to FE modelling in which the variable of interest is commonly affected by multiple model parameters, and allows for the determination of linear and non-linear effects as well as interactions between factors.

The objectives of this study were (1) to develop and validate a three-dimensional (3D) FE model of a pelvis with hip capsules intact under an anato-

Downloaded from pih.sagepub.com at UNIV TORONTO on January 12, 2012

mically neutral position using subject-specific estimates of bone geometry and location-dependent bone density, (2) to analyse pelvic strain as a function of cortical surface and interior bone density using the validated FE model, and (3) to identify and compare the high strain locations in the validated model with common insufficiency fracture sites in the pelvis as reported in the literature. It is hypothesized that the locations of high strains and those most sensitive to changes in bone density would correspond to sites prone to pelvic insufficiency fractures. While multiple factors, including geometric and material property changes as well as alterations in loading, affect mechanical resistance, quantifying the relative contributions of bone density alterations to pelvic strain is an important first step in developing a better understanding of insufficiency fracture risk.

2 METHODS

2.1 Experimental set-up

A fresh-frozen 58-year-old female pelvis (Division of Anatomy, University of Toronto) was used to develop and validate a subject-specific 3D FE model. The specimen was sectioned from the L5 vertebrae to the midshaft of both femurs. Soft tissue was removed while leaving the hip capsule, sacroiliac, iliolumbar, lumbosacral, sacrospinous, and sacrotuberous ligaments intact. A CT scan of the specimen was obtained using a GE Lightspeed Plus CT scanner (512×512 acquisition matrix, in-plane resolution 0.8×0.8 mm, slice thickness 3.2 mm, 108 slices). A bone mineral density phantom was used during the scanning procedure to enable accurate correlation of bone density with CT intensity. A total of 12 fiducials were placed on the specimen to allow for registration of the scan to the FE model and experimental set-up; fiducials were placed on the anterior superior iliac spine, posterior iliac rim, and anterior iliac rim of each hemipelvis, and three along the length of each femur.

The pelvis was mounted in an anatomically neutral double-leg stance position for testing on a MTS Bionix 858 (Eden Prairie, Minnesota) (Fig. 2). The distal femurs and L5 were potted into mounting cups using bone cement (PMMA). Strain gauges with a resistance of 120 ohm (FLA-3-11-3LT; Tokyo Sokki Kenkyujo Co. Ltd, Tokyo, Japan) were bonded to the osseous surface of the pelvis, and strains were recorded using DaqBook 2000a and DBK43-A strain gauge modules (IO-Tech, Cleveland, Ohio). Seven

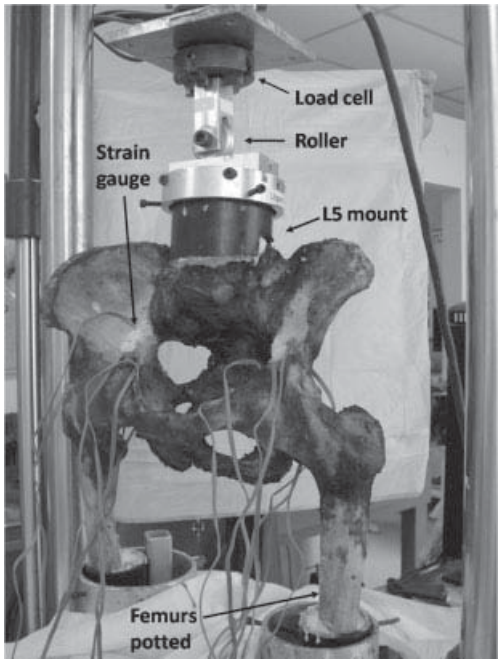

Fig. 2 Experimental set-up. The pelvis, in an anatomically neutral double-leg stance position, was loaded through L5. The roller beneath the load cell provided lateral and rotational relief

uniaxial strain gauges were placed onto each hemipelvis at approximately symmetrical locations (total of 14 gauges) (Fig. 3). Through pretesting assessment of the pelvic FE model using estimated loading and boundary conditions, areas of relatively high strain, low strain gradient, and without excessive curvature were identified to guide strain gauge placements. Strain gauge placements additionally

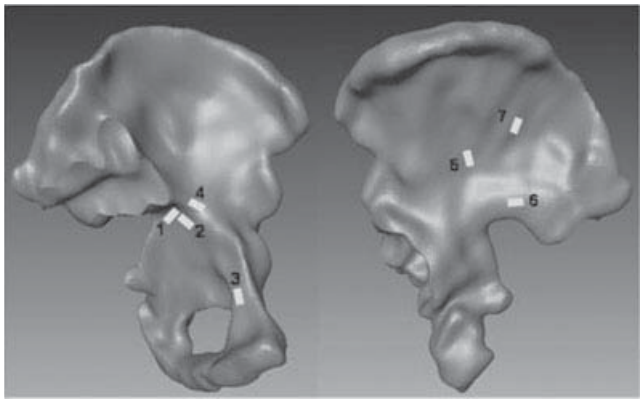

Fig. 3 Strain gauge placements shown on the left hemipelvis. A total of seven strain gauges (as shown) were placed on each hemipelvis. The strain at each location under loading conditions of 0.25, 0.50, and $0.75 \times$ body weight (500 N), applied in a stepwise manner, was obtained for six trials

Downloaded from pih.sagepub.com at UNIV TORONTO on January 12, 2012

considered similarities to locations previously utilized in the literature [**25**, **26**].

The specimen was loaded in axial compression through L5 at 0.25, 0.50, and 0.75 × body weight (500 N). The maximum load was chosen to be representative of loading under a static neutral double-leg stance position. This magnitude represents much lower load levels than would occur in active motion, but was chosen to preclude damage to the specimen during repeated testing. In order accurately to determine the axial loading direction, the angle of tilt of the L5 segment was measured relative to the vertical axis of the MTS (Microscribe 3DX; Immersion Corp., San Jose, California). The loading was applied in a stepwise manner (i.e. loads were applied consecutively without returning to baseline 0 N) and held at each level until quasi-static equilibrium was reach before data collection was performed (i.e. $< \pm 3\,\mu\varepsilon$). The loading procedure was repeated 6 times.

2.2 Geometry extraction and finite element mesh generation

A 3D volumetric tetrahedral mesh was generated from the CT scan of the specimen (Amira 3.3.1; Mercury Computer Systems Inc., Chelmsford, Massachusetts). Manual segmentation of the CT scan was performed to identify the boundaries of the iliums, sacrum, sacroiliac cartilage, symphysis pubis, acetabular cartilage, and femurs (Fig. 4). The contours were triangulated and smoothed to form a polygonal surface from which the volumetric four-noded tetrahedral mesh was created. The surface triangular elements and tetrahedral element parameters (maximum angle, maximum edge length, aspect ratio, dihedral angle, and tetrahedral ratio) were adjusted to improve the overall mesh quality and to avoid distorted tetrahedral elements of poor quality (Fig. 5).

2.3 Material properties

In the FE model, both cortical and trabecular bone were represented as isotropic linear elastic materials. CT intensity values were utilized in assigning mechanical properties for interior cortical and trabecular bone, modelled as a continuum of bony tissue [**40**]. An intensity value for each element was calculated by averaging the brightness of pixels within the element. The bone mineral density phantom established a linear relationship between the CT scanner pixel intensity (HU) and the calcium equivalent density ρ

$$\rho = 0.000\,691\,41 \times \mathrm{HU} + 1.026\,716 \tag{1a}$$

The CT intensity, measured in Hounsfield units (HU), ranged from −1000 to 3000 HU, where −1000 HU and 0 HU are the air and water equivalents respectively.

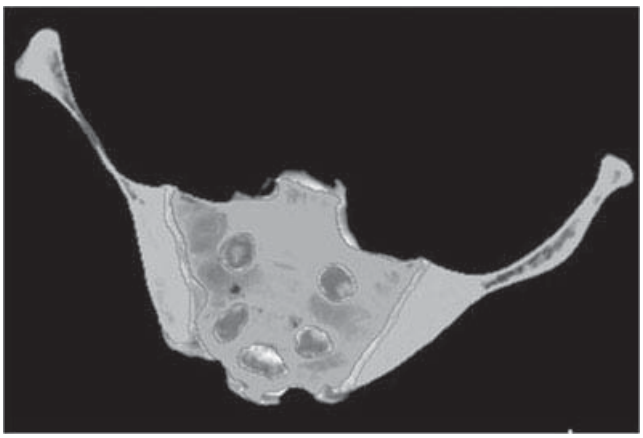

Fig. 4 CT segmentation of pelvic regions. An axial CT image slice at the level of the ilium showing the segmentation of the right ilium, left ilium, sacrum, and sacroiliac joint. The segmentation was used to generate subject-specific geometry for the FE model and to assign location-dependent material property for interior bone based on CT intensity

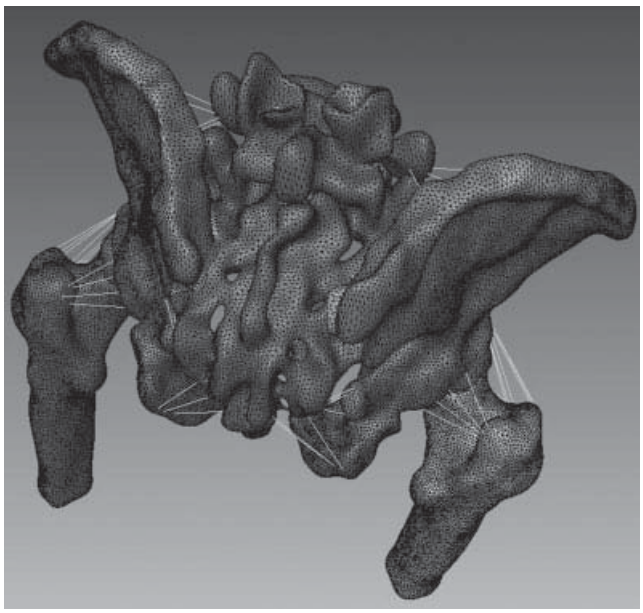

Fig. 5 Subject-specific 3D finite element model created from CT segmentation

Downloaded from pih.sagepub.com at UNIV TORONTO on January 12, 2012

It has been established that the relationship between elastic modulus and bone density is dependent on anatomic site, which may be attributed to differences in architecture [**41**]. An empirical relationship specific to pelvic bone was used to convert interior bone density to elastic modulus for each element [**42**]

$$E = 2017.3\rho^{2.46} \tag{1b}$$

where E is the elastic modulus (MPa) and ρ is the bone density (g/cm^3).

However, problems may arise in utilizing CT number in the assignment of material properties for surface elements owing to artefacts created by partial volume edge effects, resulting in an underestimation of the stiffness of affected surface tetrahedrons. Thus, the cortical bone comprising the surface elements of the pelvis was considered separately and assigned baseline material properties with a constant elastic modulus E of 17 GPa and Poisson's ratio v of 0.3 [**25**].

Ligaments of the pelvis and hip capsule were modelled as 3D two-noded non-compressible truss elements (Table 1). The stiffness value of the ligaments in compression was considered negligible. As only the mechanical properties of the iliofemoral and ischiofemoral ligaments have been reported in the literature, similar elastic modulus and Poisson's ratio values were applied to ligaments with unknown properties [**43**]. The sacroiliac joint, symphysis pubis, and a single layer of cartilage assigned to the acetabulum were modelled using a three-parameter hyperelastic Mooney–Rivlin material with coefficients of 0.1, 0.45, and 1.67 [**44**, **45**].

2.4 Boundary and loading conditions

The model was loaded evenly over all the nodes defining the L5 surface using concentrated loads applied at each node with the same magnitudes and directionality as used in the mechanical testing (0.25, 0.50, and 0.75 × body weight (500 N)). The surface interaction between the femoral head and the acetabulum was modelled as Coulomb frictional with a friction coefficient of 0.01 using a single layer of acetabular cartilage [**46**]. The femur bases were restricted from displacement in all directions to simulate the mechanical test set-up.

2.5 Data analysis

The model with the geometry, material property assignments, and boundary and loading conditions specified above was solved using non-linear static analysis in Abaqus Standard 6.6-1 (HBK, Pawtucket, Rhode Island) to produce the stress and strain distributions over the entire model. At each location in a structure, strain is a six-component tensor. However, a uniaxial strain gauge measures strain in a single direction, which corresponds to a single component of the strain tensor at that location. The coordinates of the strain gauges and the fiducial markers were digitized using a Microscribe 3DX digitizer. The position and direction of each gauge were asserted by acquiring points at the ends of the gauge, using the orientation markers on the gauge, and subsequently transformed in the model. This allowed the uniaxial strain at each gauge position with its corresponding direction to be computed within the FE model and compared against the experimental strains. The transformation of strain tensors in the direction of the corresponding strain gauge was performed using the equation

$$\varepsilon = \boldsymbol{u}^{\mathrm{T}} \Sigma \boldsymbol{u} = [u_x u_y u_z] \begin{bmatrix} \varepsilon_{xx} & \varepsilon_{xy} & \varepsilon_{xz} \\ \varepsilon_{yx} & \varepsilon_{yy} & \varepsilon_{yz} \\ \varepsilon_{zx} & \varepsilon_{zy} & \varepsilon_{zz} \end{bmatrix} \begin{bmatrix} u_x \\ u_y \\ u_z \end{bmatrix} \tag{2}$$

where ε is the strain in the direction of the strain gauge, $\boldsymbol{u}$ is the direction of the strain gauge, and Σ is the strain tensor. The error in transforming the fiducial markers used to compute the transformation between the physical space of the cadaver and the FE model was < 5 per cent. The agreement between

Table 1 Pelvis and hip capsule ligaments: mechanical properties, cross-sectional areas, and number of elements used. Ligaments were modelled as 3D two-noded non-compressible truss elements. The pelvis ligaments include sacrospinous, sacrotuberous, iliolumbar, and lumbosacral ligaments

	Elastic modulus (MPa)	Poisson's ratio	Cross-sectional area (mm^2)	Number of elements
Iliofemoral	98	0.3	98	6
Pubofemoral	98	0.3	98	3
Ligamentum teres femoris	98	0.3	73	3
Ischiofemoral	37	0.3	73	4
Pelvis ligaments	37	0.3	73	3

Downloaded from pih.sagepub.com at UNIV TORONTO on January 12, 2012

the experimentally measured strains and the extracted FE strains was assessed by the slope, offset, and r^2 value obtained from linear regression analysis.

The response surface method was used to analyse the effect of surface and interior bone density variations characterized by changes in elastic modulus. Interior and surface elastic moduli were analysed as independent variables representing bone density increases and decreases of 20 per cent from the baseline-validated model. Total maximum and minimum principal strains were the outcome-dependent variables of interest. Figure 6 shows the distribution of element elastic modulus with altered bone density at 80, 100 (baseline), and 120 per cent in the interior bone region. Elements in the cortical surface bone region with a uniform elastic modulus of 17 GPa (100 per cent) were also adjusted by $\pm$20 per cent. In the response surface model, the elastic modulus was adjusted by $\pm$10 and $\pm$20 per cent for (1) interior bone only, (2) cortical surface elements only, and (3) both interior and cortical surface bone, to obtain a uniform distribution of analyses over the solution space with a total of 25 models analysed (Design-Expert 7.7-1; Stat-Ease Inc.).

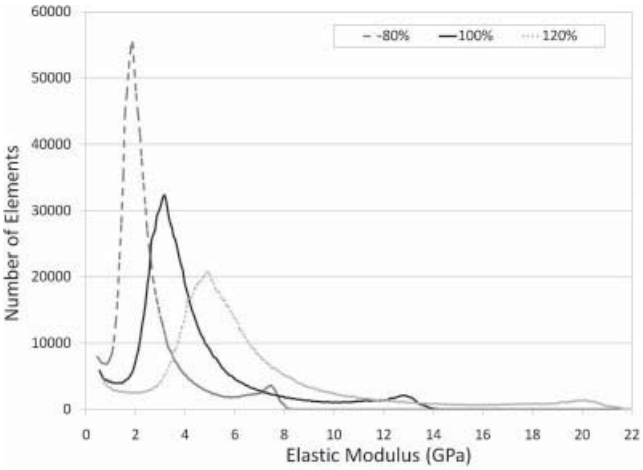

Fig. 6 Distribution of element elastic modulus at altered interior bone densities. Bone densities were altered for both cortical surface and interior bone by $\pm$20 per cent in increments of 10 per cent. The distribution of element elastic modulus with altered bone density at 80, 100, and 120 per cent in the interior bone region is shown in the graph. Elements comprising the cortical surface with a uniform elastic modulus of 17 GPa (100 per cent) were also adjusted by $\pm$20 per cent

3 RESULTS

3.1 Finite element model predictions

A convergence study was performed and the FE mesh density was accepted when the strain at each gauge location in the model changed by $< 5\,\mu\varepsilon$. The pelvis, right femur, and left femur comprised 65, 18, and 17 per cent of the final mesh, with a total of 1 226 144 first-order linear tetrahedral elements. This mesh density ensured that the minimum of three tetrahedrons through the thickness of the thin bone sections – required for a 5 per cent accuracy in modelling bending – was achieved [**24**]. The average element volume was 1.46 mm^3, which is approximately 25 per cent less than the voxel size of 1.95 mm^3; thus, the mesh density was sufficient for capturing any abrupt transitions in bone density.

The experimental strains of each gauge were averaged over the six runs for each load after adjusting for offset. However, two gauges on the right hemipelvis (gauges 1 and 4) were defective, and data were not available from them, leaving a total of 12 gauges for analysis. The standard deviation, after the highest and lowest measurements at each gauge were removed, was $< 3\,\mu\varepsilon$ at all gauges except gauge 3 on the left hemipelvis adjacent to the symphysis pubis. The gauges with the highest strains were gauges 2 and 6 on both the left and right hemipelvises.

Strain values were calculated from the FE model based on the location and direction of the experimentally placed strain gauges. High correlation was found between experimental and model strains ($r^2 = 0.93$) (Fig. 7), validating the performance of the model. The highest strain regions of the pelvis found in the model under double-leg stance loading were the greater sciatic notch, the pubic rami, the acetabular roof, and the sacral region closest to the sacroiliac joint (Fig. 8).

3.2 Bone density alterations

The validated FE model effectively simulated density alterations in the cortical surface and interior bone via the elastic modulus and its effect on strain distribution in the pelvis. Figure 9 shows the change in maximum and minimum principal strain patterns with elastic modulus adjustments from 80 to 120 per cent (a total of 40 per cent change) for interior bone only, cortical surface only, and all bone density alterations. Qualitatively, the greatest overall change in maximum and minimum principal strain was seen when both cortical surface and interior bone

Downloaded from pih.sagepub.com at UNIV TORONTO on January 12, 2012

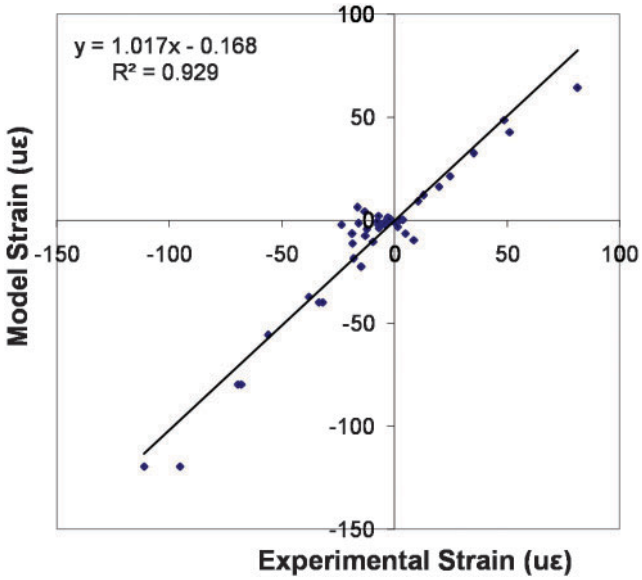

Fig. 7 Comparison of experimental versus FE model strains at all loads. Strains at gauge locations (12 in total) were validated against experimental measurements, and strong correlation was observed under all loading conditions

densities were adjusted. Changes were also noted in cortical surface only and interior only bone density alterations, with cortical surface bone density change having a larger overall impact. The increase in average principal strains for interior bone only, cortical surface only, and all bone density with a 40 per cent reduction in moduli is 2.7, 5, and 8.2 $\mu\varepsilon$ respectively. Furthermore, the regions where insufficiency fractures have been observed clinically (i.e. greater sciatic notch, pubic rami, sacral region closest to the sacroiliac joint) exhibit greater than 10 $\mu\varepsilon$ increase under all three conditions. However, it is difficult to discern by qualitatively comparing the strain patterns for interior only, cortical surface only, and all bone images (Fig. 9) whether the individual effects of cortical surface and interior bone density alterations are additive and their relative contributions to changes in strain patterns. Thus, a response surface model was used to quantify the relative impact of cortical surface and interior bone density alterations.

In altering the bone densities by $\pm$20 per cent from baseline, the total maximum and minimum principal surface strains ranged from 1.56 to 0.95 and from -1.61 to -0.97 respectively. A quadratic regression fit of the total maximum and minimum principal strains as a function of cortical surface and interior bone densities was used for the response surface model ($r^2 = 0.9991$)

$$P = u + v(A) + w(B) + x(AB) + y(A^2) + z(B^2) \tag{3}$$

where A and B denote the relative change in the surface cortical bone density and interior bone density respectively, normalized to values between 1 and -1 (0 is baseline bone density, or 100 per cent; 1 is 120 per cent; and -1 is 80 per cent), and P is the dependent variable, which is the total maximum or minimum principal strain in this study. The terms A and B describe the component of the dependence between bone density and principal strain that is linear; A^2 and B^2 describe the component of the dependence between density and principal strain that is non-linear. The term AB describes the interaction or synergistic effect that cortical surface and interior bone density together have on principal strain (i.e. the change in principal strain that would not have been present had the two densities not been altered simultaneously). Based on the value of the independent variables A and B, together with the value of the dependent variable P, for all 25 models analysed, the coefficients u, v, w, x, y, and z were solved simultaneously. The coefficient u is the intercept (baseline, $A = 0$, $B = 0$), and v, w, x, y, and z are the relative weights of each of the terms

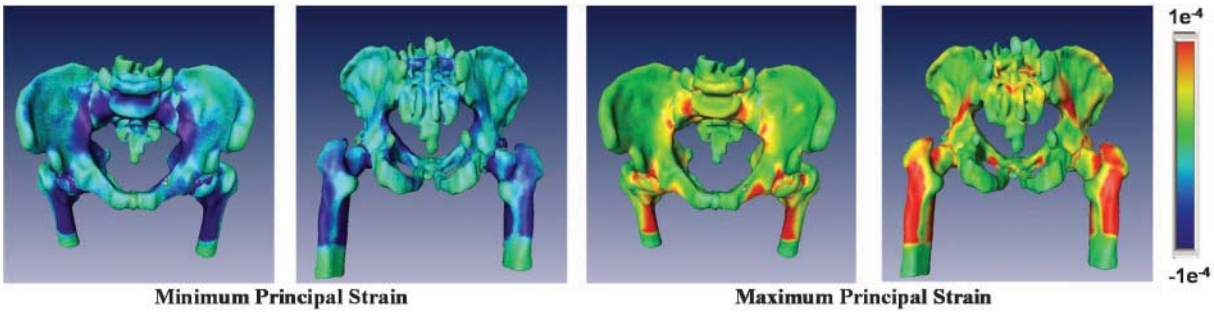

Fig. 8 Anterior and posterior views of the maximum and minimum principal strain distributions at baseline elastic modulus. Regions of high strain were found at the greater sciatic notch, the pubic rami, and the sacral region closest to the sacroiliac joint

Downloaded from pih.sagepub.com at UNIV TORONTO on January 12, 2012

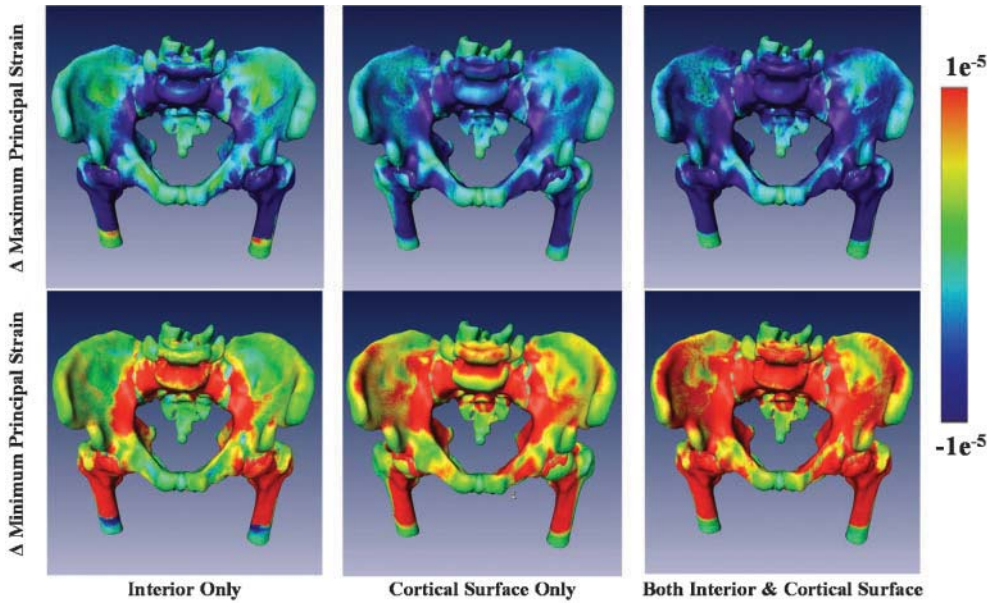

Fig. 9 Change in maximum and minimum principal strain patterns. The difference in strain pattern when bone density is adjusted from 80 to 120 per cent of baseline is shown above. Three cases were analysed, changing only interior bone density (left), changing only cortical surface bone density (middle), and changing both interior and cortical surface bone density (right). Regions of large change in compressive and tensile strains are shown in blue and red respectively, which correspond to regions prone to pelvic insufficiency fractures. The greatest overall change is seen when both bone densities are adjusted

in equation (3) (Table 2). For example, when the cortical surface density is decreased by 20 per cent ($A = -1$) and the interior bone density is at baseline ($B = 0$), the resultant maximum principal is 1.412, or an increase of 0.222 from the baseline value of 1.19. The magnitudes of the coefficients of estimates are very similar between maximum and minimum principal strains. All terms of the equation are statistically significant except for B^2, meaning that the relationship between interior bone density and principal strain is linear.

In considering the linear terms of the response surface, cortical surface bone density had a 60 per cent greater influence on the maximum and minimum principal strain compared with interior bone density. Changes of ± 20 per cent in the cortical surface density and interior bone density individually changed the principal strains by ~15 and ~9 per cent respectively. However, the principal strains changed by ~31 per cent when a decrease of 20 per cent was applied to both the cortical surface and interior bone density. There was a statistically significant but small interaction between cortical surface and interior bone density on strain (< 3 per cent). There was also a statistically significant but small non-linear effect of cortical surface bone density on strain. Overall, changes in elastic modulus had a larger effect on strain at lower densities, and the effect plateaued as bone density increased.

4 DISCUSSION

This work presents the development and successful validation of a subject-specific FE model. The strong correlation between experimental and model strains under the anatomically neutral position of a double-leg stance loaded via L5 was obtained by accurately representing the loading and boundary conditions along with inclusion of the ligaments of the hip joint and the sacrum in an intact pelvis.

As reported in the literature and summarized in Fig. 1, the common insufficiency fracture sites in the pelvis are the supra-acetabular, oblique iliac, super-

Table 2 Coefficient estimates of the response surface model for maximum and minimum principal strains

	u	v	w	x	y	z
Maximum	1.19	−0.19	−0.11	0.027	0.032	0.0048
Minimum	−1.23	0.20	0.12	−0.03	−0.032	0.0047

Downloaded from pih.sagepub.com at UNIV TORONTO on January 12, 2012

omedial iliac, superior and inferior pubic rami, and zone 1 in the sacrum, as described by Denis *et al.* [**18**]. The validated model in this study indicated that the highest strains under the double-leg stance condition occurred at the greater sciatic notch, the superior pubic rami, the supra-acetabular roof, and the region closest to the sacroiliac joint. These locations correspond to some of the pelvic sites prone to insufficiency fracture, as described in the literature, which may provide a basis for the benign loading commonly associated with this type of fracture pattern. The high strain observed near the greater sciatic notch, the acetabular roof, and the iliac region closest to the sacroiliac joint corresponds to the oblique iliac, supra-acetabular, and superomedial iliac regions described by Davis and Bradley [**15**]. In addition, the area of highest strain in the sacrum corresponded to zone 1 as described by Denis *et al.* [**18**]. Based on the loading and boundary conditions used in this study, the only site that was reported as a common insufficiency fracture site but was not identified as a region of high strain in the model was the inferior pubic ramus, whereas high strain was observed in the superior pubic ramus. This discrepancy may be due to the lack of muscle loading in this model. Alternatively, it may suggest that insufficiency fractures in the pubic rami may be due to a different loading mode in daily activities.

The regions that correspond to sites prone to insufficiency fracture were also more sensitive to changes in bone density alterations. While the increase in average maximum and minimum principal strains over the whole pelvic surface was 2.7, 5, and 8 $\mu\varepsilon$ with a 40 per cent decrease in the modulus of interior, surface, and all bone respectively, the increase in strain in areas corresponding to insufficiency fracture sites was elevated by more than 10 $\mu\varepsilon$ in all cases (Fig. 8). This indicates that these areas are particularly sensitive to density reductions, and the model is able to accurately represent focal sites for insufficiency fracture. It also demonstrates that the choice of mechanical testing configuration, the anatomically neutral double-leg stance position, is appropriate for investigating the mechanics of pelvic insufficiency fractures. While the absolute strain values reported are well below failure range, what is clinically significant is that the locations of higher strains correlate with insufficiency fracture sites. Future work may focus on correlating the magnitude of strains in these high-risk regions with the prevalence of the types of pelvic insufficiency fracture. It is common to observe multiple insufficiency fractures in the patient, and the magnitude of strain may be a common denominator between the different regions and explain their dependence.

The finding that cortical surface density has a higher impact on strain compared with interior bone density is in agreement with Anderson *et al.* [**24**], who reported that pelvis surface strains are more sensitive to changes in cortical bone elastic modulus than to changes in trabecular bone elastic modulus. While the present analysis is limited by the baseline-assigned properties of the cortical surface bone density rather than location-dependent assignment, the greater influence of cortical surface bone density is still accurate, as both the surface and interior bone were subjected to the same percentage change. In this study, the influence of cortical surface density was found to be approximately 60 per cent greater than interior bone density. The non-linear effect of the cortical surface density on strain in the present analysis means that the surface strains increase more as the modulus of these elements decreases, and as surface modulus increases the effect on strain plateaus. Thus, the impact of modulus reduction on the surface has a greater effect towards promoting insufficiency fracture risk at lower moduli. In comparison, the effect of changes in interior bone modulus on surface strains is linear. The significant but small interaction between the cortical surface and interior bone modulus means that the two parameters are not independent in their effect on strain, so that changing both moduli yields a greater impact on surface strains than merely adding the individual effects. Individually decreasing the modulus of cortical surface and interior bone by 20 per cent created an increase of 15 and 9 per cent in strain respectively; yet synergism was seen, as the change in strain from decreasing both bone moduli was 31 per cent, highlighting the small but significant interaction between the two factors. Because cortical surface density has a higher impact on strain, it may be identified as a strong global indicator for insufficiency fracture risk. However, the interaction between these bone densities as well as the non-linear effect of cortical surface bone density should also be considered in assessing insufficiency fracture risk in local bony regions, as the local strain depends on the relative amount of surface to interior bone in the region of interest. With respect to the non-linear effect of surface cortical bone density, this implies that clinicians should view bone density decreases of a patient with low bone density as more significant than decreases of a patient with relatively higher bone density. Ultimately, these findings may be incorporated into

Downloaded from pih.sagepub.com at UNIV TORONTO on January 12, 2012

an equation-based guideline once there is an agreed-upon index of insufficiency fracture risk in the field.

FE models of the pelvis have been previously used to analyse force and stresses due to muscles and ligaments acting on the hip bone as well as the dynamic behaviour of the pelvis during lateral impact [**34**–**36**]. Specific to pelvic fractures, other modelling studies have examined the mechanical stability of internal and external fixation devices for the pelvic ring and the effects of coronal pelvic inclination after hip joint surgery on insufficiency fractures [**33**, **37**]. These studies provided evidence of the appropriateness of the FE method for the study of pelvic mechanics. In addition, several studies have performed validation by matching FE analyses to experimental results, yielding good correlation with different configurations of load application [**24**–**27**]. Anderson *et al.* [**24**], Dalstra *et al.* [**25**], and Shim *et al.* [**27**] used a configuration in which the iliac crest of a hemipelvis is submerged in cement with a vertical load applied to simulate the hip joint force during a one-legged stance. In the FE validation performed by Li *et al.* [**26**] to study periacetabular defects, an intact pelvic ring was subjected to loading via the sacrum in an experimental apparatus simulating a single-leg stance. A simulated abductor muscle force was also applied via a cable pulled between the greater trochanter and iliac ring, which was designed to model the *in vivo* loading environment of the hip joint (as first described by Olson *et al.*) [**47**]. Li *et al.* [**26**] incorporated a simulated abductor load but did not capture the complexity of the origin of this muscle nor the additional musculature of the anatomy (i.e. the flexor muscles). However, the complexity in simulating the full musculature with *in vitro* experimentation is not necessary to validate an FE model. This complexity motivates the use of computational modelling as opposed to experimental testing to understand the impact of musculature on the behaviour of the pelvis. Phillips *et al.* [**48**] performed such a study and found that musculature on the pelvis functioned to distribute forces more evenly.

In the experimental set-up in this study, an entire pelvis including the sacrum, L5, and both femurs, under an anatomically neutral double-leg stance position, was loaded via L5. Ligaments were incorporated under the static loading conditions without the inclusion of muscle forces. As muscle forces remain quite limited in attempting to represent *in vivo* conditions during *in vitro* testing, this work opted to forgo the inclusion of muscle forces to facilitate the model validation. Further development of the simpler validated FE model could incorporate muscle origins, insertions, and forces [**48**, **49**]. Validation of such a configuration *in vitro* would be challenging, but similar RSM methods, as employed in this study, could be utilized to determine the sensitivity of pelvic strains to these muscle forces using the validated model as a baseline case.

In the model, a high-density tetrahedral mesh of four-node elements was utilized. The complexity of the pelvic anatomy motivates the use of automated meshing algorithms, which are optimized for tetrahedrons. A similar approach was utilized by Anderson *et al.* [**24**], who showed via mesh refinement studies that such elements can behave robustly, even in bending, if sufficient mesh density is utilized (i.e. a minimum of three tetrahedral elements through the thickness to achieve 5 per cent accuracy in capturing a beam subject to bending). Previous models have utilized hexahedral elements but have compromised either on their ability accurately to capture geometry with large elements [**3**, **25**] or on element quality in dividing up tetrahedrons into irregular hexahedral elements [**26**]. Manley *et al.* [**50**] generated a very elegant pelvic mesh of hexahedral elements to examine the impact of total hip arthroplasty on the acetabulum, but experimental validation was not carried out on this model.

A distinct division was not imposed between cortical and trabecular bone tissue in the present model, but rather the bone was modelled continuously based on its CT intensity representing density. Only cortical surface elements were assigned a distinct modulus to prevent partial volume edge effects from reducing the stiffness of surface elements and to understand the distinct impact of surface stiffness. It has been demonstrated in this study that, with sufficient element density, the continuum from cortical to trabecular bone is automatically captured with a tetrahedral mesh utilizing CT-based intensity assignments. While separate shell elements have been utilized in some models to represent cortical bone [**24**, **25**], this approach creates an artificial region of overlap between interior elements and the surface shell elements. Studies have approached this dilemma by assigning very low modulus to the base elements underlying the shell structure, but this has implications with respect to the distribution of stress and strain throughout the continuum. While these studies provided insight as to the impact of a cortical shell, the effect of surface elements alone on strain patterns has been overlooked but is also important to consider from a modelling viewpoint. The present

Downloaded from pih.sagepub.com at UNIV TORONTO on January 12, 2012

model reinforced the need to make accommodations for partial volume edge effects in utilizing subject-specific CT intensity data to describe bony material properties. An alternative to the shell elements that have been previously utilized is manual segmentation of the cortical bone and assignment of a distinct modulus to the cortical elements [**26**]. Even with high-resolution CT scans, segmentation efforts required accurately and repeatably to differentiate cortical from trabecular bone to define shell thickness are particularly difficult in thin-bone geometry. While efforts have been made to develop automated segmentation methods for thin bone structures using combinations of thresholding, smoothing filters, and level set methods, to date this approach still requires significant user intervention to address the thinnest bone regions [**51**]. The need for shell elements and segmentation of the cortical–trabecular boundary has been removed in the present model through the use of a sufficiently dense mesh. With the use of a cortical–trabecular bone continuum in the present model, the analysis was limited to quantifying the impact of cortical surface versus interior bone density changes on strain and the interaction between these parameters, rather than cortical versus trabecular bone. While the definition of a distinct cortical shell facilitates parametric variation of cortical thickness, changes in this parameter would be possible in future analyses of the present model through the identification and shifting of CT-based intensity gradients.

In the modelling process, solution convergence depended greatly on the presence of sufficient restraints specified by the boundary conditions. A pelvis resting on two femurs is an intrinsically unstable configuration, and the hip capsule ligaments serve to hold the pelvis in place. In a pilot study that excluded the ligaments of the hip capsules in the model, artificial boundary conditions, such as restricting the pelvis to vertical displacement only, were needed to obtain solution convergence; this, however, generated inaccurate strain distributions and poor correlation with experimental data ($r^2 < 0.6$). In the reported model, where ligaments were incorporated and the pelvis was allowed to move with six degrees of freedom, correlation between the model and experimental measurements improved significantly. Phillips *et al.* [**48**] established that inclusion of ligamentous boundary conditions in FE modelling of the pelvis lowered the occurrence of stress concentrations in pelvic FE models. The model used in the present study further highlights the importance of including ligaments in developing accurate FE models. However, the mechanical properties of the pelvis and hip capsule ligaments are currently not well understood, and only limited relevant data are available in the literature.

Cosson *et al.* [**52**] reported on the maximal strength for iliopectineal, sacrospinous, and arcus tendineus of pelvic fascia; however, no data were provided on the elastic modulus or cross-sectional area of the ligaments, which are required in FE modelling. However, their study did establish that there is great inter- and intrasubject variability in ligament strength. Conza *et al.* [**53**] performed vibration testing and concluded that the sacrospinous, sacrotuberous, and iliolumbar ligaments do not play a role in pelvic dynamics. However, the contribution of these ligaments in static loading has not been investigated. In the present model, the mechanical properties of the pelvic ligaments were assumed to be the same as the hip capsule ligaments. Further studies are needed to assess the sensitivity of pelvic FE models to ligament mechanical properties, origins, and insertions; an RSM approach would be suitable for such an analysis.

Accurate representation of the loading direction through L5 was also important in the validation, as it dictates the load distribution between the two hemipelvises. The mirrored gauge strains on the two hemipelvises did not correspond exactly, which suggested that loading, geometry, or material properties were not fully symmetric. In a pilot study it was observed that slight deviations in the loading direction from the vertical axis dictated whether the pelvis tilted anteriorly or posteriorly as the load was applied. When a directly vertical load was assumed in the model used for the pilot study, this resulted in a posterior tilt in the model, whereas an anterior tilt was observed in the experiment. The angle of tilt, as determined using Microscribe digitization in the experimental set-up, was applied to the FE model to ensure similarity in the axial loading direction. The correlation between model and experimental strains improved when the loading direction was adjusted according to the measured angle of tilt of the L5 segment, relative to the vertical loading direction, and it yielded an anterior tilt in the FE model as seen experimentally. Previous validation studies did not encounter similar loading direction issues, primarily because their configurations did not allow for rotational freedom between the pelvis and the femur [**24**, **26**, **47**]. This demonstrates that pelvic motion and strains are very sensitive to even slight variations in loading orientation when the experimental configuration mimics the physiological rotational free-

Downloaded from pih.sagepub.com at UNIV TORONTO on January 12, 2012

dom that exists between the pelvis and the femurs. However, once validated with accurate representation of loading direction in the experimental configuration, the FE model can be applied to study various loading vectors and their resultant strain patterns.

A maximum load magnitude of 75 per cent body weight was chosen to represent a static double-leg stance position in contrast to much higher load levels that can be experienced by the pelvis under dynamic conditions (i.e. up to 300 per cent body weight during gait) [**54**]. Limiting the load levels applied reduced the likelihood of specimen failure during testing and ensured that the strains measured at the strain gauge locations were linearly related to the magnitude of that load. As bone has been shown to fail at constant strain, irrespective of density, such strain-based analysis, which uses lower magnitudes of load for validation purposes, is justified owing to the linear behaviour within the prefailure region [**55**].

In a double-leg stance loading position, contact between the acetabulum and femoral head must be carefully defined. Contact pairs were defined through master and slave surfaces, where the harder surface, in this case the femoral head, could penetrate into the slave surface of the acetabulum. Initial penetration of the two surfaces must be eliminated by moving penetrating nodes of the slave surface; otherwise Abaqus is unable to solve the model. This causes elements that are smaller than the depth of penetration to become distorted or inverted. Obviously, this becomes increasingly problematic as the mesh becomes finer, because smaller tetrahedral elements are more susceptible to distortion by node movements. In the present study, this difficulty was addressed by careful segmentation and subsequent meshing to ensure that a small initial gap between the acetabulum and femoral head was present. A very small preload was then applied in an initial step to provide contact before the actual magnitude of load was applied.

With respect to material properties: the acetabular cartilage, the symphysis pubis, and the sacroiliac joint were modelled with three-parameter hyperelastic Mooney–Rivlin models in this study. In studies where the FE model focus is on joint mechanics and soft tissue behaviour, more complex models have been used to represent the biphasic and viscoelastic behaviour of cartilage [**56**–**58**]. Hyperelasticity represents a reasonable material assumption for FE modelling of the pelvis that incorporates joints but is focused on bony behaviour [**24**, **26**, **36**]. Future studies could perform parametric analyses to assess the impact of cartilage material properties and geometry simplifications on outcome variables.

In the validation process, strain gauge locations and directions used in testing were matched to the model. The uniaxial strain gauges utilized in this study yield specific directional measures of strain and do not provide information on in-plane surface principal strains at a given anatomic site. The uniaxial gauge locations and directions were determined, and the corresponding strains were extracted from the FE model to validate against the experimental strain measurements. The present experimental model did not attempt to make assumptions about the orientation of principal surface strains using the uniaxial gauges – rather, once validated, the FE model was used to determine the maximum and minimum principal strains over the continuum of space with respect to global coordinates.

The use of uniaxial strain gauges is a limitation in this study because only strain in a single direction is obtained at each gauge location, whereas triaxial gauges would have allowed for a more robust validation in the plane of the pelvic surface, including the minimum and maximum principal axes. However, the transformation technique used in the validation still compared strain between experimental and model results along the same direction. Some compensation for the limitation of the uniaxial gauges utilized comes from the relatively large number of strain gauges that were arranged to span across the entire pelvic surface while concentrating in regions known to undergo appreciable deformation such as the pelvic rim. As such, this study was still able to obtain an accurate model through validation using robust transformation techniques over a diverse spectrum of pelvic regions in the face of the limitations associated with uniaxial strain gauges.

The FE method is particularly appropriate for providing a biomechanical understanding of the impact of bone density alterations on insufficiency fractures. FE modelling can accommodate the complex geometry of thin bone structures such as the pelvis, where simplified geometries suitable for analytical methods cannot provide accurate solutions. It also allows for position-dependent material property assignment, which has been shown to improve model accuracy compared with using uniform material properties [**25**]. FE analysis enables visualization of strain patterns, and, when combined with position-specific bone density, high strain locations can be compared with clinically identified areas of increased insufficiency fracture risk.

Downloaded from pih.sagepub.com at UNIV TORONTO on January 12, 2012

This paper focused on the impact of bone density alone in affecting strain patterns in the pelvis. Bone density alteration was chosen as the initial factor to consider because insufficiency fracture risk has traditionally been assessed by bone density, owing to the availability of clinical methods to do so, and thus appears to be a practical starting point. However, this is only one of many factors; changes in distribution of bone (including changes in cortical bone thickness) and geometry also occur with ageing and disease [**7**–**9**]. The multiple factors in assessing insufficiency fracture risk have a common source in the interrelated remodelling processes by osteoblast and osteoclast activities. While several studies have characterized these microstructural remodelling processes, their relative importance to mechanical properties remains elusive [**59**–**61**]. At a macroscopic level, consideration of such factors is possible using FE analysis, which may provide further insight into the relative contributions of geometry and bone density to fracture risk prediction. Altering the distribution of bone will be possible with future modifications to the bone densities assigned in the present model. However, quantifying the impact of changes in pelvic geometry would require more complex changes. Mesh-morphing algorithms have been successfully used in bony structures (i.e. the vertebrae [**62**]), but the complex geometry of the pelvis would present additional challenges in focusing analyses and assessing the impact of geometric changes.

Response surface methods have been widely used in different fields to identify the independent effects of multiple factors on an outcome variable, yet its use in biomechanical FE modelling has been limited. This investigation provides a proof-of-concept of the ability of the response surface method effectively to identify the relative contributions of cortical surface and interior bone densities, non-linearity effects, as well as the interaction between these bone densities to surface strains. It provides more information than traditional sensitivity analyses, as the interaction of factors can be identified. One shortcoming of the response surface method is that it can be time consuming and computationally intensive to perform multiple analyses over the entire solution space. However, most statistical software provides power calculations, which generate the least number of analyses needed to obtain the desired power. Future efforts in FE modelling could be directed at automating the generation of response surface models.

In conclusion, the high-density tetrahedral FE model presented in this work shows excellent correlation with experimental testing data. The sophistication of this model came with the inclusion of specimen-specific material properties, pelvic and hip capsule ligaments, and an anatomically neutral loading condition representing a double-leg stance. Strain patterns in the model corresponded to areas of clinical incidence of insufficiency fracture, and the response surface method was shown to be useful in quantifying the relative contributions of cortical surface and interior bone density to pelvic strains. Information on the relative influence of multiple parameters in an FE model derived from a response surface model may lead to the development of more accurate models by focusing modelling efforts on the parameters with the greatest influence. Future studies in this area could investigate the effects of changes in the distribution (thickness) of cortical bone, geometric variations, and additional loading and boundary conditions (including muscle loading) on pelvic mechanics. Comparisons of FE model strain patterns with more specific quantitative clinical data on pelvic regions with high risk of insufficiency fractures could ultimately establish a better understanding of the relationship between pelvic structural parameters and insufficiency fracture risk.

ACKNOWLEDGEMENT

This project was funded by the National Science and Engineering Research Council of Canada.

© Authors 2009

REFERENCES

1 **Tile, M.** Pelvic ring fractures: should they be fixed? *J. Bone Jt Surg. Br.*, 1988, **70**(1), 1–12.
2 **Jacob, H. A., Huggler, A. H., Dietschi, C.,** and **Schreiber, A.** Mechanical function of subchondral bone as experimentally determined on the acetabulum of the human pelvis. *J. Biomechanics*, 1976, **9**(10), 625–627.
3 **Dalstra, M.** and **Huiskes, R.** The pelvic bone as a sandwich construction: a three dimensional finite element study. *Proc. ESB*, 1990, **7**, B32.
4 **Pentecost, R. L., Murray, R. A.,** and **Brindley, H. H.** Fatigue, insufficiency and pathologic fractures. *JAMA*, 1964, **187**, 1001–1004.
5 **Daffner, R. H.** and **Pavlov, H.** Stress fractures: current concepts. *AJR Am. J. Roentgenol.*, 1992, **159**(2), 245–252.
6 **Silva, M. J.** Biomechanics of osteoporotic fractures. *Injury – Int. J. Care Injured*, 2007, **38S3**, S69–S76.

Downloaded from pih.sagepub.com at UNIV TORONTO on January 12, 2012

7 **Uusi-Rasi, K., Sievänen, H., Pasanen, M.,** and **Kannus, P.** Age-related decline in trabecular and cortical density: a 5-year peripheral quantitative computed tomography follow-up study of pre- and postmenopausal women. *Calcif. Tissue Int.*, 2007, **81**(4), 249–253.

8 **Russo, C. R., Lauretani, F., Bandinelli, S., Bartali, B., Di Iorio, A., Volpato, S., Guralnik, J. M., Harris, T.,** and **Ferrucci, L.** Aging bone in men and women: beyond changes in bone mineral density. *Osteoporos. Int.*, 2003, **14**(7), 531–538.

9 **Riggs, B. L., Melton III, L. J., Robb, R. A., Camp, J. J., Atkinson, E. J., Peterson, J. M., Rouleau, P. A., McCollough, C. H., Bouxsein, M. L.,** and **Khosla, S.** Population-based study of age and sex differences in bone volumetric density, size, geometry, and structure at different skeletal sites. *J. Bone Miner. Res.*, 2004, **19**(12), 1945–1954.

10 **Beason, D. P., Dakin, G. J., Lopez, R. R., Alonso, J. E., Bandak, F. A.,** and **Eberhardt, A. W.** Bone mineral density correlates with fracture load in experimental side impacts of the pelvis. *J. Biomechanics*, 2003, **36**(2), 219–227.

11 **Snedeker, J. G., Walz, F. H., Muser, M. H., Schroeder, G., Mueller, T. L.,** and **Müller, R.** Microstructural insight into pedestrian pelvic fracture as assessed by high-resolution computed tomography. *J. Biomechanics*, 2006, **39**(14), 2709–2713.

12 **Glüer, C. C., Cummings, S. R., Pressman, A., Li, J., Glüer, K., Faulkner, K. G., Grampp, S.,** and **Genant, H. K.** Prediction of hip fractures from pelvic radiographs: the study of osteoporotic fractures. The Study of Osteoporotic Fractures Research Group. *J. Bone Miner. Res.*, 1994, **9**(5), 671–677.

13 **Iglič, A., Srakar, F.,** and **Antolic, V.** Influence of the pelvic shape on the biomechanical status of the hip. *Clin. Biomechanics*, 1993, **8**, 223–224.

14 **Soubrier, M., Dubost, J. J., Boisgard, S., Sauvezie, B., Gaillard, P., Michel, J. L.,** and **Ristori, J. M.** Insufficiency fracture. A survey of 60 cases and review of the literature. *Joint Bone Spine*, 2003, **70**(3), 209–218.

15 **Davies, A. M.** and **Bradley, S. A.** Iliac insufficiency fractures. *Br. J. Radiol.*, 1991, **64**(760), 305–309.

16 **Schapira, D., Militeanu, D., Israel, O.,** and **Scharf, Y.** Insufficiency fractures of the pubic ramus. *Semin. Arthritis Rheum.*, 1996, **25**(6), 373–382.

17 **Isdale, A. H.** Stress fractures of the pubic rami in rheumatoid arthritis. *Ann. Rheum. Dis.*, 1993, **52**(9), 681–684.

18 **Denis, F., Davis, S.,** and **Comfort, T.** Sacral fractures: an important problem. Retrospective analysis of 236 cases. *Clin. Orthop. Related Res.*, 1988, **227**, 67–81.

19 **Schindler, O. S., Watura, R.,** and **Cobby, M.** Sacral insufficiency fractures. *J. Orthop. Surg.*, 2007, **15**(3), 339–346.

20 **Weber, M., Hasler, P.,** and **Gerber, H.** Insufficiency fractures of the sacrum: twenty cases and review of the literature. *Spine*, 1993, **18**(16), 2507–2512.

21 **Grangier, C., Garcia, J., Howarth, N. R., May, M.,** and **Rossier, P.** Role of MRI in the diagnosis of insufficiency fractures of the sacrum and acetabular roof. *Skeletal Radiol.*, 1997, **26**(7), 517–524.

22 **Lin, J. T.** and **Lane, J. M.** Sacral stress fractures. *J. Women's Health*, 2003, **12**(9), 879–888.

23 **Tsiridis, E., Upadhyay, N.,** and **Giannoudis, P. V.** Sacral insufficiency fractures: current concepts of management. *Osteoporos. Int.*, 2006, **17**(12), 1716–1725.

24 **Anderson, A. E., Peters, C. L., Tuttle, B. D.,** and **Weiss, J. A.** Subject-specific finite element model of the pelvis: development, validation and sensitivity studies. *ASME J. Biomech. Engng*, 2005, **127**(3), 364–373.

25 **Dalstra, M., Huiskes, R.,** and **van Erning, L.** Development and validation of a three-dimensional finite element model of the pelvic bone. *ASME J. Biomech. Engng*, 1995, **117**(3), 272–278.

26 **Li, Z., Butala, N. B., Etheridge, B. S., Siegel, H. J., Lemons, J. E.,** and **Eberhardt, A. W.** A biomechanical study of periacetabular defects and cement filling. *ASME J. Biomech. Engng*, 2007, **129**(2), 129–136.

27 **Shim, V. B., Pitto, R. P., Streicher, R. M., Hunter, P. J.,** and **Anderson, I. A.** Development and validation of patient-specific finite element models of the hemipelvis generated from a sparse CT data set. *ASME J. Biomech. Engng*, 2008, **130**(5), 051010.

28 **Keyak, J. H., Fourkas, M. G., Meagher, J. M.,** and **Skinner, H. B.** Validation of an automated method of three-dimensional finite element modelling of bone. *J. Biomed. Engng*, 1993, **15**(6), 505–509.

29 **Maurel, N., Diop, A.,** and **Grimberg, J.** A 3D finite element model of an implanted scapula: importance of a multiparametric validation using experimental data. *J. Biomechanics*, 2005, **38**(9), 1865–1872.

30 **Gupta, S., van der Helm, F. C., Sterk, J. C., van Keulen, F.,** and **Kaptein, B. L.** Development and experimental validation of a three-dimensional finite element model of the human scapula. *Proc. IMechE, Part H: J. Engineering in Medicine*, 2004, **218**(2), 127–142. DOI: 10.1243/095441104322984022.

31 **Barker, D. S., Netherway, D. J., Krishnan, J.,** and **Hearn, T. C.** Validation of a finite element model of the human metacarpal. *Medical Engng Phys.*, 2005, **27**(2), 103–113.

32 **Hipp, J. A., McBroom, R. J., Cheal, E. J.,** and **Hayes, W. C.** Structural consequences of endosteal metastatic lesions in long bones. *J. Orthop. Res.*, 1989, **7**(6), 828–837.

33 **García, J. M., Doblaré, M., Seral, B., Seral, F., Palanca, D.,** and **Garcia, L.** Three-dimensional finite element analysis of several internal and external pelvis fixations. *ASME J. Biomech. Engng*, 2000, **122**(5), 516–522.

34 **Goel, V. K.** and **Svensson, N. L.** Forces on the pelvis. *J. Biomechanics*, 1977, **10**(3), 195–200.

Downloaded from pih.sagepub.com at UNIV TORONTO on January 12, 2012

35 **Goel, V. K., Valliappan, S.,** and **Svensson, N. L.** Stresses in the normal pelvis. *Comput. in Biol. Med.*, 1978, **8**(2), 91–104.

36 **Dawson, J. M., Khmelniker, B. V.,** and **McAndrew, M. P.** Analysis of the structural behaviour of the pelvis during lateral impact using the finite element method. *Accid. Analysis Prev.*, 1999, **31**(1–2), 109–119.

37 **Kaku, N., Tsumura, H., Taira, H., Sawatari, T.,** and **Torisu, T.** Biomechanical study of load transfer of the pubic ramus due to pelvic inclination after hip joint surgery using a three-dimensional finite element model. *J. Orthop. Sci.*, 2004, **9**(3), 264–269.

38 **Gupta, S.** and **Manohar, C. S.** An improved response surface method for the determination of failure probability and importance measures. *Structural Safety*, 2004, **26**(2), 123–139.

39 **Huang, Y. Y., Wu, S. M.,** and **Wang, C. Y.** Response surface method: a novel strategy to optimize iontophoretic transdermal delivery of thyrotropin-releasing hormone. *Pharm. Res.*, 1996, **13**(4), 547–552.

40 **Taddei, F., Pancanti, A.,** and **Viceconti, M.** An improved method for the automatic mapping of computed tomography numbers onto finite element models. *Medical Engng Phys.*, 2004, **26**(1), 61–69.

41 **Morgan, E. F., Bayraktar, H. H.,** and **Keaveny, T. M.** Trabecular bone modulus–density relationships depend on anatomic site. *J. Biomechanics*, 2003, **36**(7), 897–904.

42 **Dalstra, M., Huiskes, R., Odgaard, A.,** and **van Erning, L.** Mechanical and textural properties of pelvic trabecular bone. *J. Biomechanics*, 1993, **26**(4–5), 523–535.

43 **Hewitt, J. D., Glisson, R. R., Guilak, F.,** and **Vail, T. P.** The mechanical properties of the human hip capsule ligaments. *J. Arthroplasty*, 2002, **17**(1), 82–89.

44 **Li, Z., Alonso, J. E., Kim, J. E., Davidson, J. S., Etheridge, B. S.,** and **Eberhardt, A. W.** Three-dimensional finite element models of the human pubic symphysis with viscohyperelastic soft tissues. *Ann. Biomed. Engng*, 2006, **34**(9), 1452–1462.

45 **Dakin, G. J., Arbelaez, R. A., Molz IV, F. J., Alonso, J. E., Mann, K. A.,** and **Eberhardt, A. W.** Elastic and viscoelastic properties of the human pubic symphysis joint: effects of lateral impact joint loading. *ASME J. Biomech. Engng*, 2001, **123**(3), 218–226.

46 **McLeish, R. D.** and **Charnley, J.** Abduction forces in the one-legged stance. *J. Biomechanics*, 1970, **3**(2), 191–209.

47 **Olson, S. A., Bay, B. K.,** and **Hamel, A.** Biomechanics of the hip joint and the effects of fracture of the acetabulum. *Clin. Orthop. Related Res.*, 1997, **339**, 92–104.

48 **Phillips, A. T. M., Pankaj, P., Howie, C. R., Usmani, A. S.,** and **Simpson, A. H.** Finite element modelling of the pelvis: inclusion of muscular and ligamentous boundary conditions. *Medical Engng Phys.*, 2007, **29**(7), 739–748.

49 **Dalstra, M.** and **Huiskes, R.** Load transfer across the pelvic bone. *J. Biomechanics*, 1995, **28**(6), 715–724.

50 **Manley, M. T., Ong, K. L.,** and **Kurtz, S. M.** The potential for bone loss in acetabular structures following THA. *Clin. Orthop. Related Res.*, 2006, **453**, 246–253.

51 **Szwedowski, T. D.** *Development and validation of a subject-specific finite element model of the craniofacial skeleton*. MASc Thesis, Institute of Biomaterials and Biomedical Engineering, University of Toronto, Toronto, Ontario, 2007.

52 **Cosson, M., Boukerrou, M., Lacaze, S., Lambaudie, E., Fasel, J., Mesdagh, H., Lobry, P.,** and **Ego, A.** A study of pelvic ligament strength. *Eur. J. Obstet. and Gynecol. and Reprod. Biol.*, 2003, **109**(1), 80–87.

53 **Conza, N. E., Rixen, D. J.,** and **Plomp, S.** Vibration testing of a fresh-frozen human pelvis: the role of pelvic ligaments. *J. Biomechanics*, 2007, **40**(7), 1599–1605.

54 **Bergmann, G., Deuretzbacher, G., Heller, M., Graichen, F., Rohlmann, A., Strauss, J.,** and **Duda, G. N.** Hip contact forces and gait patterns from routine activities. *J. Biomechanics*, 2001, **34**(7), 859–871.

55 **Kopperdahl, D. L.** and **Keaveny, T. M.** Yield strain behavior of trabecular bone. *J. Biomechanics*, 1998, **31**(7), 601–608.

56 **Ehlers, W.** and **Markert, B.** A linear viscoelastic biphasic model for soft tissue based on the theory of porous media. *ASME J. Biomech. Engng*, 2001, **123**, 418–424.

57 **Almeida, E. S.** and **Spilker, R. L.** Finite element formulations for hyperelastic transversely isotropic biphasic soft tissue. *Comput. Meth. in Appl. Mechanics and Engng*, 1998, **151**, 513–538.

58 **Suh, J. K.** and **Bai, S.** Finite element formulation of biphasic poroviscoelastic model for articular cartilage. *ASME J. Biomech. Engng*, 1998, **120**, 195–201.

59 **Brockstedt, H., Kassem, M., Eriksen, E. F., Mosekilde, L.,** and **Melsen, F.** Age- and sex-related changes in iliac cortical bone mass and remodeling. *Bone*, 1993, **14**, 681–691.

60 **McCalden, R. W., McGeough, J. A., Barker, M. B.,** and **Court-Brown, C. M.** Age-related changes in the tensile properties of cortical bone. The relative importance of changes in porosity, mineralization, and microstructure. *J. Bone Jt Surg. Am.*, 1993, **75**(8), 1193–1205.

61 **Augat, P., Reeb, H.,** and **Claes, L. E.** Prediction of fracture load at different skeletal sites by geometric properties of the cortical shell. *J. Bone Miner. Res.*, 1996, **11**(9), 1356–1363.

62 **Sigal, I. A., Hardisty, M. R.,** and **Whyne, C. M.** Mesh-morphing algorithms for specimen-specific finite element modeling. *J. Biomechanics*, 2008, **41**(7), 1381–1389.

Downloaded from pih.sagepub.com at UNIV TORONTO on January 12, 2012